Photochemical age determinations in the Phoenix metropolitan area

L. I. Kleinman,[1] P. H. Daum,[1] Y.-N. Lee,[1] L. J. Nunnermacker,[1] S. R. Springston,[1] J. Weinstein-Lloyd,[2] P. Hyde,[3] P. Doskey,[4] J. Rudolph,[5] J. Fast,[6] and C. Berkowitz[6]

Received 5 June 2002; revised 3 September 2002; accepted 6 September 2002; published 5 February 2003.

[1] An extensive VOC data set was gathered as part of a photochemical oxidant field campaign conducted in the Phoenix air basin in the late spring of 1998. Sampling was done at the surface and by aircraft at midboundary layer height; in regions with emission sources and downwind in the urban plume. VOC concentration ratios were used to calculate photochemical age, defined as the time integrated exposure of an air mass to OH radical. Based on the VOC ratios of 15 compounds (with OH reactivity varying between acetylene and p, m-xylene), we present estimates for photochemical age and dilution factors for several regions within the air basin. Geographic trends are in agreement with the expectation that pollutants are transported in a generally eastward direction so that older and more dilute mixtures occur to the east of the city. Photochemical ages determined from aircraft samples agree with those determined at a downwind surface site. The bias in photochemical age that occurs because fresh pollutants are added to an aged mixture has been quantified by using a particle trajectory model. A combination of trajectory results (actual age of the pollutants in an air mass) and photochemical age yields an estimate of the average OH concentration experienced by the air parcel. OH obtained in this way is somewhat lower, but has the same trends as OH concentrations calculated using a photochemical box model that is constrained with observed concentrations coincident with the VOC samples. *INDEX TERMS:* 0345 Atmospheric Composition and Structure: Pollution—urban and regional (0305); 0365 Atmospheric Composition and Structure: Troposphere—composition and chemistry; 0368 Atmospheric Composition and Structure: Troposphere—constituent transport and chemistry; *KEYWORDS:* Photochemical age, hydrocarbons, urban plume, urban photochemistry, photochemistry, Phoenix

Citation: Kleinman, L. I., et al., Photochemical age determinations in the Phoenix metropolitan area, *J. Geophys. Res.*, *108*(D3), 4096, doi:10.1029/2002JD002621, 2003.

1. Introduction

[2] During May and June of 1998, the Atmospheric Chemistry Program of the DOE in collaboration with the Arizona Department of Air Quality (ADEQ) conducted a photochemical oxidant measurement campaign in the Phoenix metropolitan area. This region experiences elevated O_3 with peak values occasionally greater than 120 ppb [*EPA*, 2000]. Distinguishing features of the Phoenix air basin are complex wind patterns due to the surrounding terrain, very low humidity, high temperature and solar insulation, a high mixing height, and an emissions mixture dominated by mobile sources. Meteorological and chemical conditions in Phoenix thereby offer an interesting contrast to urban areas outside of the arid Southwest, which have been more extensively studied [*Solomon et al.*, 2000]. The Phoenix campaign involved aircraft sampling by the DOE G-1 and a surface network of chemical and meteorological stations. Participants in this study included researchers from the ADEQ, Argonne National Laboratory (ANL), Brookhaven National Laboratory (BNL), Pacific Northwest National Laboratory (PNNL), SUNY, Old Westbury, and York University.

[3] Aircraft flights were designed to sample the urban plume at various points in its evolution. The simple picture that guided our flight plans was that an air mass would pick up fresh pollutants over the downtown urban area; photochemical processing and mixing would occur as the plume was advected away from its source region; and eventually the air mass would lose its distinctive chemical features and merge into a regional background. This picture works quite well as a foundation for the analysis of field data in the circumstance when there is a plume from a well-defined source region advected in a simple flow field. Thus, for

[1]Atmospheric Sciences Division, Brookhaven National Laboratory, Upton, New York, USA.
[2]Chemistry/Physics Department, SUNY/Old Westbury, Old Westbury, New York, USA.
[3]Arizona Department of Environmental Quality, Phoenix, Arizona, USA.
[4]Argonne National Laboratory, Environmental Research Division, Argonne National Laboratory, Argonne, Illinois, USA.
[5]Chemistry Department and Centre for Atmospheric Research, York University, Toronto, Ontario, Canada.
[6]Pacific Northwest National Laboratory, Atmospheric Science Department, Richland, Washington, USA.

0148-0227/03/2002JD002621$09.00

example, urban and power plant plumes sampled in the Nashville SOS field campaign were often analyzed in terms of air mass evolution [*Cowling et al.*, 1998, 2000, and references therein].

[4] The situation in Phoenix is more complex. Airflows in the Phoenix basin are affected by terrain induced heating and cooling that set up a basin-wide circulation that often dominates the synoptic weather pattern [*Ellis et al.*, 1999]. The Phoenix metropolitan area is also large, so that an air mass traversing the region can have fresh emissions added on top of emissions that have already undergone a significant amount of photochemical processing.

[5] In this study we use a photochemical age technique to determine the degree of processing in an air mass. This technique depends on the fact that more reactive chemicals are consumed faster than less reactive ones, so that as an air mass ages there are systematic changes in concentration ratios. In addition to a differential effect based on reactivity, all concentrations tend to decrease with time as air from a source region becomes diluted with cleaner background air. By using volatile organic compounds (VOCs) that react almost exclusively with OH radical, changes in a concentration ratio can provide quantitative information on the time-integrated exposure of the air mass to OH radical. This quantity, $[OH]_{AVG} \times$ time, is called photochemical age. Since many chemical processes are sensitive to OH, photochemical age is a useful overall measure of where an air mass is in the aging continuum between fresh emissions at one end and a depleted background-like condition at the other end.

[6] Many researchers over the last 25 years have used VOC ratios to determine photochemical age [*Calvert*, 1976; *Roberts et al.*, 1984; *Rudolph and Johnen*, 1990; *McKeen et al.*, 1990, 1996; *Parrish et al.*, 1992; *Satsumabayashi et al.*, 1992; *Blake et al.*, 1993; *McKeen and Liu*, 1993; *McKenna et al.*, 1995; *McKenna*, 1997; *Volz-Thomas and Kolahgar*, 2000; *Rudolph and Czuba*, 2000]. In the process a great deal has been learned about the conditions that have to apply in order to obtain useful information. These are discussed in a following section. Here we briefly note that photochemical age is not necessarily a well-defined quantity because the actual age (time since emission) of the various VOCs in an air parcel can and do differ. Photochemical age has been likened to a clock that can be inappropriately reset to a low age if fresh, reactive emissions are added to an older air mass [*Parrish et al.*, 1992]. This is a concern in a region such as Phoenix with a spatially extended emissions area.

[7] Our objectives for this study are three-fold: First, to determine how photochemical age varies over the Phoenix air basin. Second, to quantify the degree to which VOC ratios underestimate photochemical age because of the large area covered by emission sources. For this purpose we use the PNNL particle trajectory model [*Fast and Berkowitz*, 1996; *Fast et al.*, 2000] to simulate the age dispersion of VOCs collected in the aircraft samples. Third, to compare 2 estimates of OH concentration. This is a qualitative exercise because the combination of particle trajectories and photochemical age yields an average OH experienced by an air mass, while a photochemical box model constrained by observations [*Kleinman et al.*, 1997] yields a calculated OH concentration for the trajectory end-point.

2. Experimental

[8] Phoenix is a city of 1.2 million people located in a metropolitan area having a total population of 3 million people. The Phoenix air basin is defined by mountains to the west, north, and east. The topography of the region and NO_x emission rate are shown in Figure 1. Emissions are mainly due to area sources and follow the geographic distribution of people and highways. There are no large electric generation plants within the metropolitan area. Because most emissions are due to mobile sources [*Heisler et al.*, 1997], the relative proportions of NO_x and VOC emissions are to a first approximation similar throughout the basin.

[9] The Phoenix campaign included aircraft sampling and a network of surface monitoring sites, many of which had augmented instrumentation and sampling schedules. Figure 1 shows sites located in Downtown Phoenix and to the east in the Usery Mountain Pass. The Downtown "Super Site" is in a high-density source region. Early morning observation there should be indicative of unprocessed emissions. The site at Usery Pass is in a region where a mature urban plume with high O_3 levels was expected [*Doskey et al.*, 2000; *Gaffney et al.*, 2002]. Between 18 May and 10 June, the G-1 conducted 24 research flights. Figures 2a and 2b show typical midmorning (AM) and afternoon flight patterns (PM). The AM pattern was usually conducted between 0800 and 1100, mostly within the growing convective boundary layer. The PM pattern was usually flown between 1430 and 1700, near the time at which peak O_3 levels were expected. All times are local standard time (LST) equal to UTC - 7. Vertical profiles to an altitude of at least 3000 m were made on both AM and PM flights. The AM flights covered regions that were nominally upwind of Phoenix while the PM flights covered regions to the east in the nominally downwind direction. In both AM and PM flights sampling was done over the main emission source region.

2.1. VOC Data Sets

[10] Five to ten VOC canisters were usually filled on each flight. Locations of samples discussed in this paper are shown in Figures 2a and 2b, for the AM and PM flights, respectively. Each sample is indicated as a single point, but it took about 30 s to fill a canister, which translates into a 3 km distance at the 100 m s^{-1} cruising speed of the G-1. Several screening criteria were applied to the G-1 VOC data set to arrive at the points shown in Figures 2a and 2b. The first criteria are geographic location and time of day, which yielded the groupings "West" and "Urban AM" for morning samples and "Urban PM," "East," and "Mountain" for afternoon samples. Note that the Urban samples include some that were taken over low emission rate regions in addition to ones taken over very high emission rate regions, as shown in Figure 1. Source-like samples will be defined in a subsequent section according to concentration. All samples used for photochemical age determinations were within the convective boundary layer at an altitude below 2000 m. Low concentrations of the less reactive VOCs were observed in the morning at high altitude ($\approx$3000 m), above

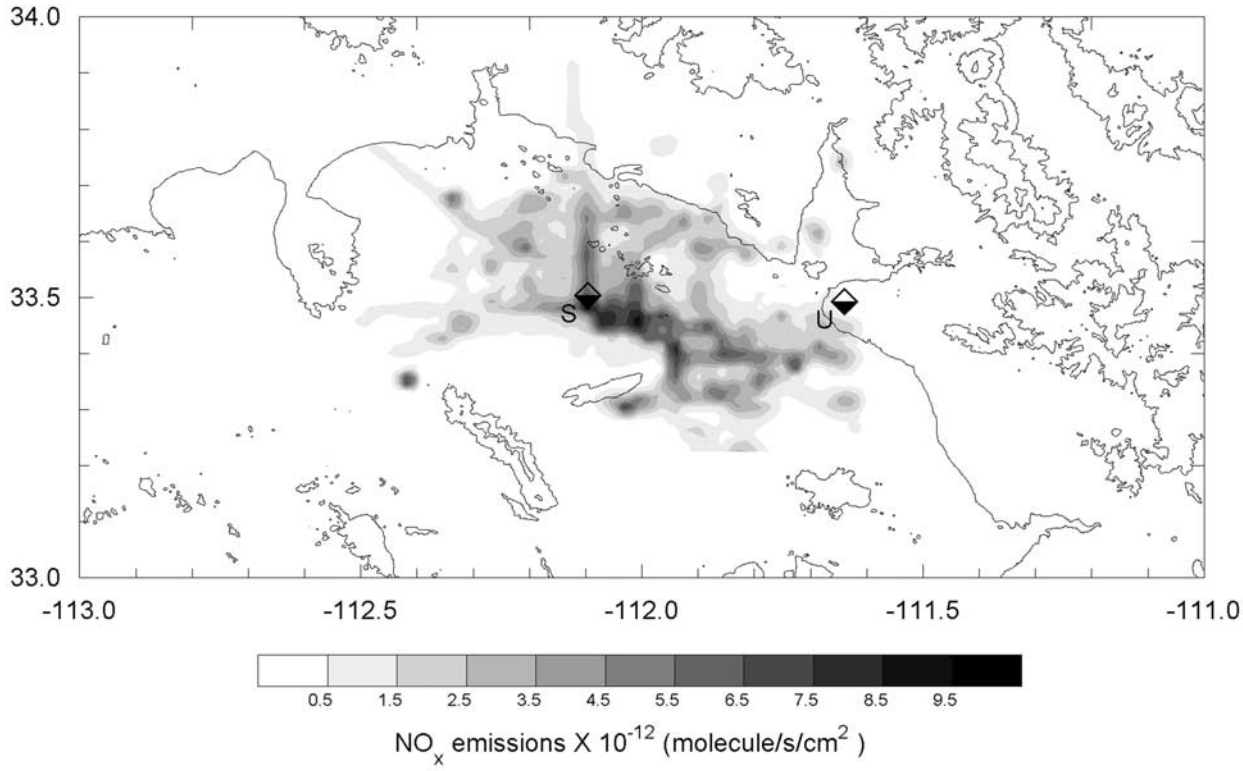

Figure 1. Map of Phoenix area, showing topography, NO_x emission rate at 0900, and surface chemistry sites. Contour lines are drawn at 500 m intervals. Diamonds labeled with "S" and "U" show locations of the Downtown Super Site and the site at Usery Pass.

the boundary layer. These measurements were used to determine an average background, which was subtracted from the boundary layer G-1 observations. This subtraction has only a small effect on photochemical age determinations and was done primarily because the particle trajectory model was not run in a mode that would allow this background to be calculated.

[11] VOC data collected by ANL at Usery Pass was available for 4 days in May. On each day, 8 three-hour integrated samples were taken covering a diurnal cycle. The ADEQ conducted VOC sampling at 4 locations including the downtown "Super Site." Source categorization will be based on 11 two-hour integrated morning samples collected between 0700–0900 at the Super Site.

2.2. VOC Collection and Analysis

[12] VOC samples from the G-1 were collected in 3 liter SUMMA® electro-polished stainless steel canisters and analyzed at York University. Principles and details of the gas chromatographic procedures are described by *Rudolph* [1999], *Rudolph and Khedim* [1985], and references therein. All samples were analyzed on two different GC-FID systems. In both instruments the VOCs in the samples are enriched from typically 1 dm^3 of air by a two-step cryogenic preconcentration. Light hydrocarbons (C_2–C_7) are separated on an aluminum oxide porous layer open tubular (PLOT) column (30 m, 0.32 mm I.D. C_4–C_{10} hydrocarbons were analyzed on a GC equipped with a 60m DB-1 column (0.25 mm I.D., 1 μm film thickness). Peak identification is based on retention time. Retention times are established and regularly checked by running synthetic mixtures; peak assignments were verified by cochromatography. Measurements were evaluated quantitatively by comparison with a ppb-level mixture of approximately 120 hydrocarbons in synthetic air. The lower limit of detection for completely resolved peaks is nominally 1 ppt. The reproducibility of the measurements as determined from repeat analysis of randomly selected samples, is between 2% and 5%. For mixing ratios near the lower limit of detection (low ppt range), the uncertainties increase to between 10% and 30%. Accuracy of the measurements is estimated to be approximately 10% or better as confirmed by the results of several intercomparisons, including the Nonmethane Hydrocarbon Intercomparison Experiment [*Apel et al.*, 1994, 1999]. However, for light alkenes, an artifact of several ppt is formed in the type of canisters used in this study [e.g., *Ramacher et al.*, 1997].

[13] Air samples taken at Usery Pass by ANL were cryogenically preconcentrated with a Chemical Data Systems (CDS) 330 sample concentrator (Autoclave Inc., Oxford, PA) and were analyzed with a Hewlett-Packard 5890A high-resolution gas chromatograph (Palo Alto, CA) with a flame ionization detector (FID) by an analytic technique described in detail by *Fukui and Doskey* [1996]. Sampling at Usery Pass is described in *Doskey et al.* [2000]. Briefly, the whole-air samples were preconcentrated at −100°C in a 15-cm section of a glass-lined stainless steel tube (0.180 cm ID) packed with 60/80 mesh

porous glass beads (Unibeads 1S; Alltech Associates, Inc., Deerfield, IL). The preconcentrated samples were thermally desorbed at 100°C for 2 min and were transferred to either (1) a 60-m × 0.32-mm-ID fused-silica capillary column coated with a 1-μm-thick film of polydimethylsiloxane (DB-1; J&W Scientific, Folsom, CA) or (2) a 30-m × 0.53-mm-ID porous-layer open tubular column coated with alumina (GS-Alumina; J&W Scientific, Folsom, CA). The FID was calibrated daily with a mixture of C_2-C_6 *n*-alkanes, benzene, and toluene at a level of 10 ppb each (Scott Specialty Gases, Inc., Plumsteadville, PA).

[14] VOC samples from the downtown Super Site were collected and analyzed by the Desert Research Institute under the auspices of the ADEQ. Samples were collected in 6 liter SUMMA® electro-polished stainless steel canisters. The sampling and analysis procedure follows that recommended by the Environmental Protection Agency [*EPA*, 1991]. An air sample from the pressurized canister is concentrated on a freeze-out loop and then transferred to a Hewlett-Packard 5890 Series II gas chromatograph, equipped with FID and ECD detectors. The chromatographic column is a 60 m long fused silica capillary column with a 0.32 mm inside diameter and 1 μm phase thickness. The GC/FID response is calibrated in parts per billion carbon (ppbc), using primary calibration standards traceable to the National Institute of Standards and Technology Standard Reference Materials. Analysis is for C_2-C_{12} hydrocarbons and halogenated hydrocarbons. Selected samples are reanalyzed by the gas chromatography/Fourier transform infrared/mass spectrometry (GC/FTIR/MS) technique to confirm the identification of individual hydrocarbons. Identification of individual components is based on their retention times and mass and infrared spectra matching those of authentic standards.

3. Photochemical Age: Method

[15] At the point of emission, VOCs have characteristic concentration ratios depending on the type of emission source. Downwind of a source, concentration ratios change as the more reactive compounds are preferentially removed by oxidation. Reaction loss depends on photochemical age, defined as the time integrated exposure to OH radical with time being marked from the point of emission to the point at which observations are made. In addition, concentrations decrease due to dilution with background air. In the idealized case, VOCs are emitted into the atmosphere from a single source location; reaction is only with OH radical; transport is nondiffusive so that there is a unique well-defined travel time; and background air has a negligible VOC concentration [*Rudolph and Johnen*, 1990]. According to these simplifying assumptions, the concentration of VOCs i and j are given by

$$C_i(t) = D(t)C_i(0)\exp(-k_i[OH]t) \quad (1)$$

$$C_j(t) = D(t)C_j(0)\exp\left(-k_j[OH]t\right), \quad (2)$$

where D(t) is a dilution factor, $C_i(0)$ is an initial concentration, the k's are rate constants for reaction with OH, and t is the travel time from emission source to receptor. Note that low values of D correspond to air masses that are more dilute. A dilution factor and photochemical age can be obtained from (1–2):

$$\ln D(t) = \left[k_j \ln(C_i(t)/C_i(0)) - k_i \ln\left(C_j(t)/C_j(0)\right)\right]/\left(k_j - k_i\right) \quad (3)$$

$$[OH]t = \left[\ln(C_i(t)/C_i(0)) - \ln\left(C_j(t)/C_j(0)\right)\right]/\left(k_j - k_i\right). \quad (4)$$

In cases where an independent estimate of time is available, equation (4) can be used to determine OH radical concentration [see, e.g., *Roberts et al.*, 1984; *Blake et al.*, 1993; *McKenna et al.*, 1995; *Volz-Thomas and Kolahgar*, 2000].

[16] There is a rich literature describing the theory and practice of photochemical age calculations. A paper by *McKeen et al.* [1990] summarizes many of the pre-1990 determinations of [OH] noting that the underlying assumption that transport and chemistry are independent (i.e., can be written in the product form of (1–2)) is often not valid. A coupling between transport and chemistry occurs because (1) a single unique travel time does not exist, either because sources are spatially extended or because diffusion smears an air parcel so that part of it travels faster than the mean and part travels slower, and (2) the exponential factors in (1–2) give more weight to sources that are nearby in time. Thus a reactive VOC will, on average, have traveled a shorter time to the receptor than a less reactive VOC. As a consequence, photochemical age is underestimated, with the error becoming larger when more reactive VOCs are used. This problem has been treated quantitatively by obtaining analytic and numerical solutions to reaction — diffusion equations [*McKeen et al.*, 1990; *McKenna*, 1997; *Ehhalt et al.*, 1998; and *Rudolph and Czuba*, 2000]. From these studies it is known that the criteria for a successful application of (3–4) is that

$$\left|k_i - k_j\right|[OH]\Delta t < 1, \quad (5)$$

where Δt is a characteristic spread in travel times caused by the geographic distribution of emission sources and/or atmospheric diffusion. When photochemical age calculations are done for different pairs of VOCs, it has been found that as $|k_i - k_j|$ increase, age predictions decrease [*Roberts et al.*, 1984; *Blake et al.*, 1993].

[17] In this study rather than considering pairs of VOCs, we will use a set of 15 VOC measurements in a single age determination by doing a linear regression of $\ln(C_i(t)/C_i(0))$ versus k_i [*Volz-Thomas and Kolahgar*, 2000]. The slope of the regression is -[OH]t and the intercept is ln (D(t)). The advantages of simultaneously considering a large set of VOCs are several fold: Anomalous concentrations measurements due to unusual source characteristics or measurement error are apparent as outliers on a regression plot. Trends in photochemical age with reactivity are apparent as curvature of the data points on the regression. Random measurement errors tend to cancel because the regression in effect is providing an average age and dilution from many pairs of compounds [*McKenna et al.*, 1995]. As we will be combining VOC observations from the G-1 and surface sites, issues of measurement consistency are important and will be addressed in a following section. NO_x and NO_y could also be used in determining photochemical age,

either by adding NO_2 to the list of VOCs or by following changes in NO_x/NO_y. This approach was not pursued because NO_2 at the Downtown surface site was not directly measured.

3.1. Choice of VOCs

[18] Several criteria have to be met by the VOCs used in the regression analysis: Concentrations should be relatively high to aid in accurate quantification. The reactivity range has to be wide enough so that $C_i(t)/C_i(0)$ can be readily distinguished from $C_j(t)/C_j(0)$ but not so wide that (5) no longer applies. Background concentrations should be relatively low and compounds should be characteristic of the main emission categories.

[19] Table 1 lists the compounds used in our analysis. The top part of the list, consisting of compounds with k's below 2×10^{-11} molec cm^{-3} s follows a listing of the most abundant VOCs in the G-1 samples excluding ethane because of its high background and excluding several compounds that were not quantified in at least 90% of the samples. Propane was excluded because of the episodic occurrence of extremely high values in the Downtown surface samples. Reactive olefins, with k's $\geq 2.6 \times 10^{-11}$ molec cm^{-3} s, were used only for determining the age of a set of high concentration G-1 samples relative to the Downtown surface measurements. This restriction was applied to avoid violating the reactivity limit specified by (5). Even without (5), the use of reactive olefins in low concentration samples is problematic due to formation of artifact alkenes in the type of canisters used for this study. A similar anomaly was found by *McKenna et al.* [1995] who noted the presence of significant concentrations of reactive hydrocarbons far downwind of an emission source.

3.2. Choice of Reference Sample

[20] Equations (3) and (4) give a photochemical age and a dilution factor relative to whatever sample is selected as a t = 0 reference point. The choice of a t = 0 sample is quite arbitrary. It need not be freshly emitted, nor is it necessary that it represent the starting point for the actual time evolution of an air parcel. Although the choice of a zero age and unit dilution factor are arbitrary, once chosen the calculations are self consistent, that is, photochemical ages and dilution factors have unique values independent of the pathway used to do the calculation. For example, suppose VOC samples have been collected at locations A, B, and C. We can directly calculate the age and dilution factor of C relative to A. This calculation, instead, could be done in 2 steps by relating B to A and then C to B. In order to get unique results that agree with the properties of age and dilution factor as expressed in equations (3) and (4), we require that ages be combined by addition and dilution factors by multiplication. In our example, age and dilution factor are related to each other by

$$\mathrm{Age}(A \rightarrow C) = \mathrm{Age}(A \rightarrow B) + \mathrm{Age}(B \rightarrow C) \quad (6)$$

$$D(A \rightarrow C) = D(A \rightarrow B) \times D(B \rightarrow C). \quad (7)$$

Note that (6) and (7) do not depend on having a particular sample chosen as a t = 0 reference point. In Section 6 we will show by numerical example that the above relations are satisfied to within a few percent.

Table 1. VOCs and Hydroxyl Radical Rate Constants Used for Photochemical Age Calculations

Compound	k(OH)[a], cm^3 $molec^{-1}$ s^{-1}
Acetylene	9.12(−13)
Benzene	1.23(−12)
Iso-Butane	2.35(−12)
n-Butane	2.56(−12)
2-Methylbutane	3.90(−12)
n-Pentane	3.97(−12)
2-Methylpentane	5.60(−12)
n-Hexane	5.61(−12)
3-Methylpentane	5.70(−12)
Toluene	5.96(−12)
Ethylbenzene	7.10(−12)
Cyclohexane	7.54(−12)
Ethene	8.44(−12)
o-Xylene	1.37(−11)
p,m-Xylene[b]	2.05(−11)
Propene[c]	2.60(−11)
Iso-Butene	5.08(−11)
cis-2-Butene	5.58(−11)
trans-2-Butene	6.32(−11)
cis-2-pentene	6.50(−11)
trans-2-pentene	6.70(−11)

[a]Rate constant for reaction with OH at 298K from *Atkinson* [1994]. The notation 9.12(−13) is meant to be read as 9.12×10^{-13}.

[b]Variable. Table value is for a weighted average for m-xylene and p-xylene in a 2:1 mixture. Reaction rate constant used in photochemical age determination varied between 2.03(−11) and 1.93(−11) according to changes in the m-xylene to p-xylene ratio as a sample ages. An iterative process was used to determine the m-xylene to p-xylene ratio consistent with photochemical age in each group of samples.

[c]Olefins other than ethene are referred to in the text as "reactive olefins."

4. Models

4.1. Particle Trajectory Model

[21] Transport and dispersion of emissions was investigated using the PNNL particle trajectory model [*Fast and Berkowitz*, 1996]. This model uses meteorological fields at a 2.5 km horizontal grid spacing obtained from the Regional Atmospheric Modeling System (RAMS) to simulate advection and turbulent diffusion. A description of the application of RAMS for the Phoenix field campaign is given in *Fast et al.* [2000]. RAMS employed a four-dimensional data assimilation technique to limit forecast errors by incorporating hourly wind speed and direction measurements from three radar wind profilers.

[22] Nonreactive particles are released near ground level at a rate proportional to NO_x emissions in the Phoenix air basin. The emission inventory has hourly resolution for a representative weekday and has 2 km by 2 km spatial resolution in the high emission rate areas [*Heisler et al.*, 1997]. Particle calculations were done for 8 days with releases starting at 0500 of each day. Calculations were originally done for another purpose, which accounts for the particle release rate being proportional to NO_x rather than VOCs. However, according to the inventory, these rates are, to a first approximation, proportional. Depending on time of day and on species, the r^2 correlation between NO_x and VOC emission rate is generally between 0.7 and 0.8.

[23] Particle calculations keep track of the number and age of particles in the volume of model space corresponding

Table 2. Average Characteristics of Hydrocarbon Samples

Location	Time, LST [a]	No.	Alt, m[b]	VOCs, ppbC[c]	O_3, ppb	NO_x, ppb
Surface Downtown[d]	0700–0900	11		217 ± 92		
Surface Usery Pass[d]	1500–1600	13		28 ± 11		
G-1 West	0906	8	917	9 ± 3	56	2.2
G-1 Urban 1st Quartile[e]	1038	15	880	61 ± 17	55	20
G-1 Urban 2nd Quartile[e]	1017	16	1020	29 ± 6	54	8.7
G-1 Urban 3rd Quartile[e]	1028	15	973	21 ± 6	57	4.8
G-1 Urban 4th Quartile[e]	1005	15	952	11 ± 5	58	2.5
G-1 Urban PM	1541	30	980	21 ± 10	65	4.4
G-1 East	1620	15	1194	12 ± 4	75	2.0
G-1 Mountain	1645	7	1779	10 ± 5	70	1.3

[a]Sampling duration for surface samples. Average time of G-1 data subset.
[b]Above mean sea level. Higher terrain in East and Mountain regions accounts for higher sample altitudes.
[c]Sum of identified compounds with standard deviation. Background from 4 high altitude morning samples is 3.9 ± 0.9 ppbC and is mostly ethane. Values in table are before background subtraction.
[d]ADEQ.
[e]Quartiles are defined according to C_2H_2 concentration as described in text.

to the position of the G-1 at the times that VOC samples were collected. In order to generate reasonable statistics we used a sampling volume that is 5 km by 5 km in the horizontal and 500 m in the vertical, centered on the G-1 location. The number of particles in this size sampling volume will be referred to as a particle concentration. Ages were grouped into 30 minute bins.

4.2. Constrained Steady State (CSS) Photochemical Model

[24] A photochemical box model was used to calculate the OH concentration that is in equilibrium with the observed mixture of stable trace gases. The model uses a chemical mechanism based on *Stockwell et al.* [1990] and *Paulson and Seinfeld* [1992]. Photolysis rate constants were calculated using programs from *Madronich* [1987]. Inputs to this model are observed or estimated values for O_3, NO, CO, VOCs, HCHO, H_2O_2, organic peroxides, H_2O, solar intensity, temperature, and pressure. Concentrations were averaged over the approximately 30s time period of a VOC sample, unless the sampling period coincided with an instrument zero procedure, in which case an additional minute was added to the averaging period. Calculations were performed for all VOC samples subject to the availability of O_3, NO, and state parameters. Missing data for the other substances was handled as follows: HCHO was set to a calculated steady state value and peroxides were estimated based on their correlation with O_3 and dew point. Further information on the photochemical calculations and the observations upon which they are based can be found in *Kleinman et al.* [1997].

5. Observations

[25] Table 2 lists characteristics of VOC samples taken from the G-1 and from the surface sites. Note that in Table 2 and elsewhere VOC concentrations are given in ppbv (parts per billion by volume of compound) when referring to an individual compound and ppbC (parts per billion by volume of carbon) when referring to a mixture of VOCs. Concentrations of other trace species and physical parameters were obtained by averaging over the time period used in collecting a VOC sample. Some G-1 VOC samples were collected while the trace gas instruments were in zero mode or otherwise unavailable, so the number of samples contributing to those averages is typically 10% fewer than the number of VOC samples. Quartile subsets of the Urban AM samples were defined according to the concentration of C_2H_2, a common vehicle exhaust product with a relatively long lifetime, which is well correlated with most other VOCs. C_2H_2 varied from 1–1.7 ppbv in the high concentration first quartile (see Figure 2) to 0.18–0.36 ppbv in the low concentration fourth quartile. Quartile subsets of the Urban AM samples will be referred to as Urban 1st Quartile, Urban 2nd Quartile, etc.

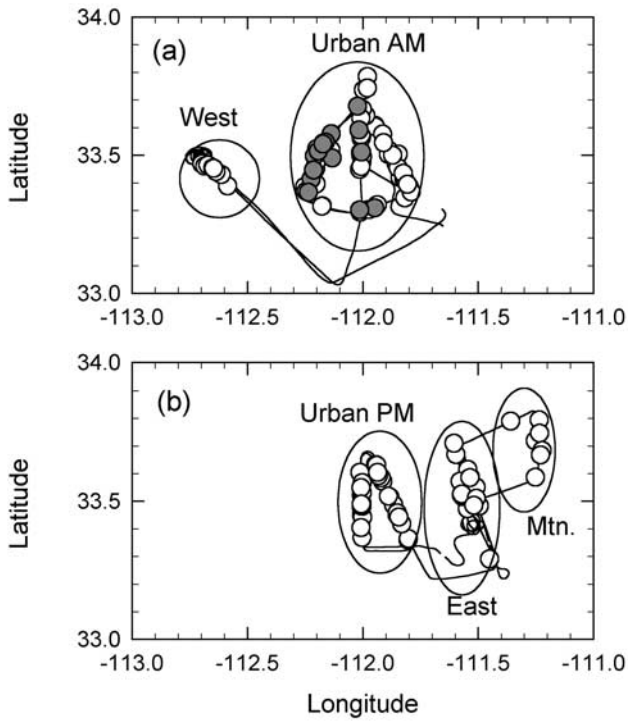

Figure 2. Map of Phoenix area showing typical flight pattern and locations of VOC samples used for photochemical age calculations (a) in the morning and (b) in the afternoon. Data has been screened for location, altitude, and VOC characteristics as discussed in text. Data subsets are defined on plots. Shaded symbols are high concentration Urban 1st Quartile samples, defined in text.

[26] A key assumption in the calculation of photochemical age is that surface and aircraft samples are capturing VOCs that originate from a similar mixture of emissions sources. A change in concentration ratio from one sample to the next can then be interpreted in terms of a differential OH exposure rather than being due to a different source signature. VOC emissions in Phoenix are dominated by mobile sources making Phoenix a favorable location for photochemical age calculations. However, a subset of the G-1 samples had a significant admixture of olefins and aromatics, unlike that found in vehicular emissions. Figure 3 illustrates this feature by showing the relation between toluene, a common solvent, and C_2H_2, a marker for vehicle exhaust. Most samples have a toluene to C_2H_2 ratio within a narrow band of values with a scatter consistent with a variable exposure to OH. A subset of the G-1 samples, some with an extremely high toluene concentration, are outliers to the main trend. Outliers were treated in one of 2 ways. Six samples had concentration anomalies in 3 or more species and were not used for the photochemical age calculations. Some of these samples were geographically clustered supporting the premise that they are from an atypical emission source. Five samples had high toluene concentration, but were otherwise normal as judged by ratios of other species. For these samples, photochemical age regressions were done without toluene. In a similar fashion, the G-1 data set was screened for atypical concentrations of other species, resulting in the removal of 1% of the individual VOC determinations. An additional 2 samples from the West grouping were not used because concentrations approached those observed in background air.

[27] In order to judge the consistency of the G-1 and surface data sets we compared concentration ratios of compounds that were either unreactive or that had similar OH reaction rate constants [*Parrish et al.*, 1998]. For this comparison we used the Urban 1st Quartile G-1 samples as these were the closest to being freshly emitted. For some pairs of compounds such as benzene/acetylene and ethylbenzene/toluene, the G-1 and surface data sets agreed within their standard deviations and furthermore agreed with the US urban averages reported by *Parrish et al.* [1998]. In other cases such as i-butane/n-butane and alkane/acetylene there were 25–50% discrepancies between G-1 and Downtown surface samples. Discrepancies could be due to differences in analysis procedures or different mixtures of emission sources. We will refer to these differences as ''measurement noise'' bearing in mind that these relatively small differences could be due to geographic variations in emission sources. Measurement noise will be quantified as an uncertainty in regression slope in the photochemical age calculations.

6. Photochemical Age: Results

[28] We report photochemical age and dilution factors for the G-1 and Usery Pass samples using an average of the 0700 Downtown surface samples as the t = 0 reference point. The downtown samples, taken in a region with high emissions and at a time of day when minimal photochemical processing occurs, are expected to have an actual age close to zero. By assigning these samples a dilution factor of unity, we are defining a concentration scale where everything is measured relative to a specific but arbitrary standard. Photochemical ages and dilution factors were also calculated using an average of the G-1 Urban 1st Quartile samples as the t = 0 reference point. Reactive olefins were only useful for determining the age of the G-1 Urban 1st Quartile samples relative to the surface.

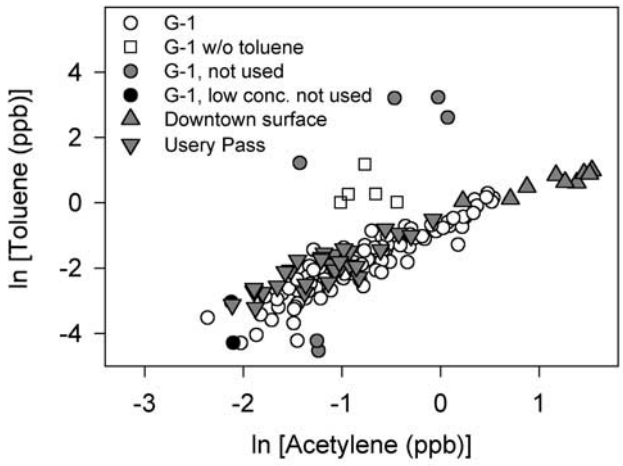

Figure 3. Relation between toluene and acetylene concentration for aircraft and surface samples. Square symbols indicate G-1 samples in which toluene was the only concentration outlier. These samples were included in our analysis but without toluene. Gray and black circles are G-1 samples, which were not used because of multiple concentration anomalies or near background concentrations, respectively.

[29] Photochemical ages and dilution factors are reported in Table 3. All of the quantitative results in this and other tables are obtained by doing a regression of $\ln(C_i(t)/C_i(0))$ versus k_i for each VOC sample in a subset. A photochemical age and dilution factor are obtained for each sample from the slope and intercept of the regression fit. These are then averaged to yield a photochemical age and dilution factor for that subset. Examples are provided in a following section. An alternate approach was used for a single figure (Figure 6). In that case, in order to illustrate the behavior of an entire data subset, VOC concentrations were first averaged and then a single regression was used to determine a dilution factor and photochemical age. The combination of analysis errors and geographic differences in source signature, described as ''measurement noise'' in the preceding section, causes an uncertainty in photochemical age, according to the regression statistics, of about 25–30%, with extremes of 9 and 51% for the Urban 1st Quartile, calculated with and without reactive olefins.

[30] Figures 4a and 4b illustrate the geographic and temporal dependencies of photochemical age and dilution. Overall, the G-1 samples show a qualitative tendency for photochemical age and dilution to be inversely related. Error bars denote the standard deviation within a data subset and provide one measure of sample-to-sample variability. It is seen that dilution factors are highly variable (standard deviation/mean = 0.5 or greater) except for the Urban quartiles, which were defined on the basis of C_2H_2 concentration and therefore by construction are relatively homoge-

Table 3. Photochemical Age and Dilution Factors for G-1 Data Sets Relative to Morning Downtown Surface Samples[a]

Data Subset[b]	Dilution Factor	Photochemical Age,[c] molec cm^{-3} s	Correlation, r^2
West	0.051	1.26(11) ± 2.5(10)	0.57
Urban 1st Quartile (with reactive olefins)	0.40	2.40(10) ± 2.9(9)	0.86
Urban 1st Quartile	0.40	2.35(10) ± 1.2(10)	0.24
Urban 2nd Quartile	0.19	3.81(10) ± 1.2(10)	0.45
Urban 3rd Quartile	0.12	4.64(10) ± 1.5(10)	0.41
Urban 4th Quartile	0.058	8.10(10) ± 2.1(10)	0.51
Urban PM	0.12	4.95(10) ± 1.7(10)	0.40
East	0.088	1.05(11) ± 2.0(10)	0.65
Mountain	0.068	1.29(11) ± 2.8(10)	0.62

[a]Downtown surface samples by definition have a dilution factor of 1.0 and a photochemical age of 0.
[b]Age, dilution, and correlation calculated for each sample in a data set. Values presented here are averages of these individual determinations.
[c]The notation 1.26(11) is meant to be read as 1.26×10^{11}. The second number is a standard error of the regression slope.

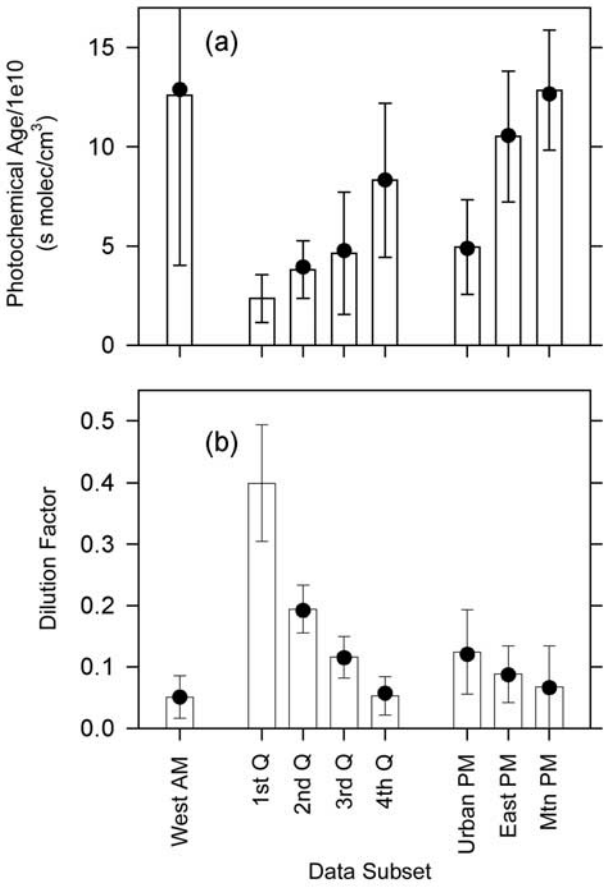

Figure 4. (a) Photochemical age and (b) dilution factor for G-1 data subsets as given in Table 3. Bars show average value for a data subset and error bars give the standard deviation. Regression calculations were done using the Downtown 0700 surface samples as a t = 0 reference point, that is, the surface samples have a photochemical age of 0 and a dilution factor of 1. Calculations were repeated using the G-1 Urban 1st Quartile samples as a t = 0 reference point. Ages and dilution factors from those calculations were combined with the age and dilution factor of the Urban 1st Quartile subset relative to the surface samples using equations (6) and (7). Results given by solid circles.

neous in concentration. Recall that the dilution factor is simply a measure of concentration relative to the downtown surface site. A factor less than 1 can be due to the dilution of downtown air with clean background air or be due to a source region with a low emission rate. Taken as a group the Urban AM samples vary from being source-like in the 1st Quartile to resembling an aged dilute VOC mixture in the 4th Quartile. In the afternoon, samples tend to be more aged and dilute as the distance from the city center increases in the sequence Downtown, East, and Mountain. Upwind morning samples in the West are among the oldest and most dilute.

[31] Equations (6) and (7), which show how photochemical ages and dilution factors can be combined, are tested in Figures 4a and 4b. Photochemical ages were determined by adding the age of the G-1 1st Quartile subset to an age calculated relative to the 1st Quartile. In a similar fashion, dilution factors were combined by multiplication. Values, so obtained, agree with values calculated directly to within a few percent; it is difficult to see the differences on the graphs.

[32] A diurnal cycle for photochemical age at the Usery Pass surface site is shown in Figure 5. There is a pro-

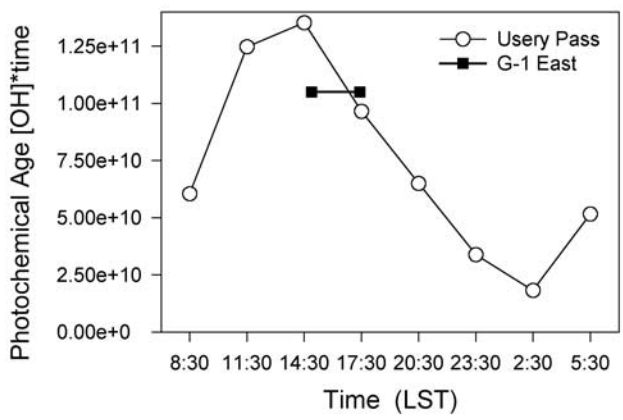

Figure 5. Diurnal cycle of photochemical age at Usery Pass. Open circle data points are located at the midpoint of a 3-hour sample collection interval. Circles are connected with straight lines for visual clarity. The G-1 data shows the average photochemical age of the East sample subset and the time range over which those samples were collected.

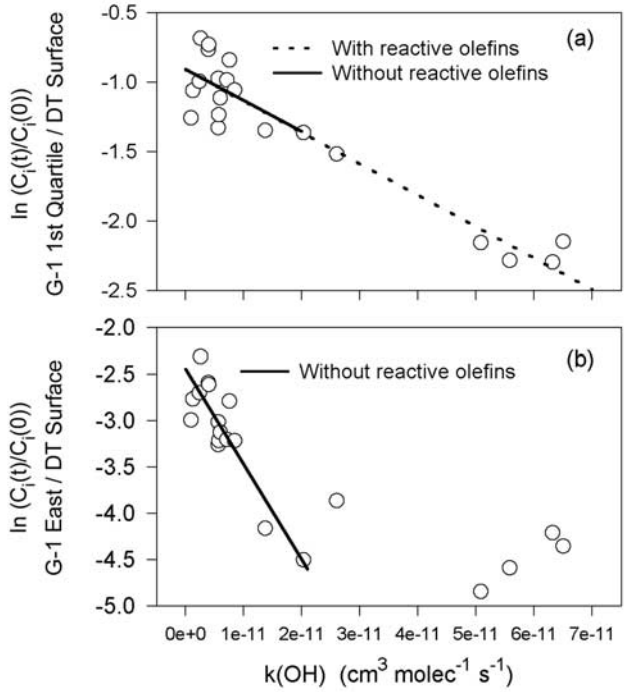

Figure 6. Photochemical age regression plots of ln (VOC ratio) versus OH reaction rate constant. (a) Regression used to determine age of a composite G-1 Urban 1st Quartile sample relative to the Downtown 0700 surface observations. Composite G-1 sample is an unweighted average of 15 samples. Downtown concentrations are an average of 11 samples. A linear least squares fit was done with and without reactive olefins. Regressions parameters are D = 0.40, photochemical age = 2.22×10^{10} s cm^{-3}, and r^2 = 0.20 without reactive olefins; D = 0.40, photochemical age = 2.26×10^{10} s cm^{-3}, and r^2 = 0.90 with reactive olefins. (b) Regression used to determine age of a composite G-1 East sample relative to the Downtown 0700 surface observations. Regression parameters are D = 0.087, photochemical age = 1.03×10^{11} s cm^{-3}, and r^2 = 0.80. A data point for t-2-pentene is off-scale, low. Values in Table 3 differ because the table was constructed by averaging over regressions for individual samples.

nounced difference between well-aged pollutants in the late morning and early afternoon versus the source-like material seen in the very early morning. *Doskey et al.* [2000] have noted the same feature based on the abundance of olefins and on the ratio of toluene to benzene. Their analysis indicates that VOCs at Usery Pass resemble vehicle emissions that have undergone varying amounts of photochemical processing. The relatively unreacted material observed at 2330 and 0230 could be emissions from the evening rush hour transported from the major sources regions to the west (see Figure 1). As *Doskey et al.* [2000] and *Gaffney et al.* [2002] have noted, plumes with high concentrations of NO_2 and VOCs were often observed at that hour. The increase in age for the 0400 to 0700 time period is consistent with nocturnal drainage winds transporting aged pollutants from the Superstition Mountains to the east back toward the city. The G-1 flight track for the East samples was within a few km of Usery Pass and Figure 5 indicates that samples collected on the ground in the late afternoon have the same photochemical age as those collected 1km above ground level.

6.1. Examples

[33] We have chosen 4 examples, presented in Figures 6 and 7, to illustrate features of the photochemical age methodology and the Phoenix data set. The first 2 examples illustrate characteristics of reactive olefins and measurement noise. The next 2 examples show regressions that cover a wide range of photochemical age.

[34] Figure 6a shows a photochemical age determination for a composite Urban 1st Quartile sample with and without reactive olefins. Data points without reactive olefins ($k < 2 \times 10^{-11}$ molec cm^{-3} s) are quite scattered (r^2 = 0.20). A much better fit (r^2 = 0.90) is obtained from the regression that uses reactive olefins. Visually it appears that the information content of Figure 6a is contained primarily in the selective disappearance of reactive olefins. Both regressions, however, have nearly identical slopes and intercepts as quantified in the figure caption. This agreement is

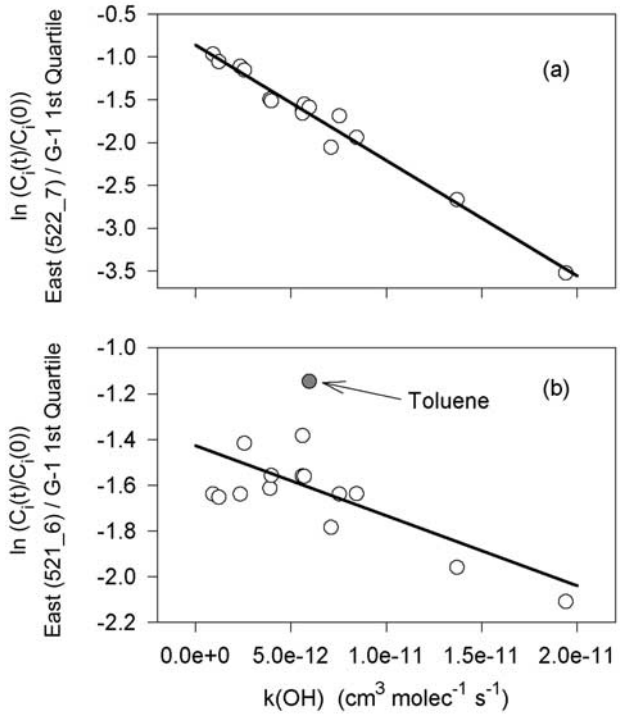

Figure 7. Photochemical age regression plots of ln (VOC ratio) versus OH reaction rate constant applied to determining the age of a single East sample relative to the Urban 1st Quartile observations. (a) 22 May, sample #7. Straight line is the linear least squares fit excluding reactive olefins. Regression parameters are D = 0.43, photochemical age = 1.35×10^{11} s cm^{-3}, and r^2 = 0.98. (b) 21 May, sample #6. Straight line is a linear least squares fit including a data point for toluene. Regressions parameters are D = 0.24, photochemical age = 3.06×10^{10} s cm^{-3}, and r^2 = 0.43 with toluene; D = 0.23, photochemical age = 3.02×10^{10} s cm^{-3}, and r^2 = 0.63 without toluene.

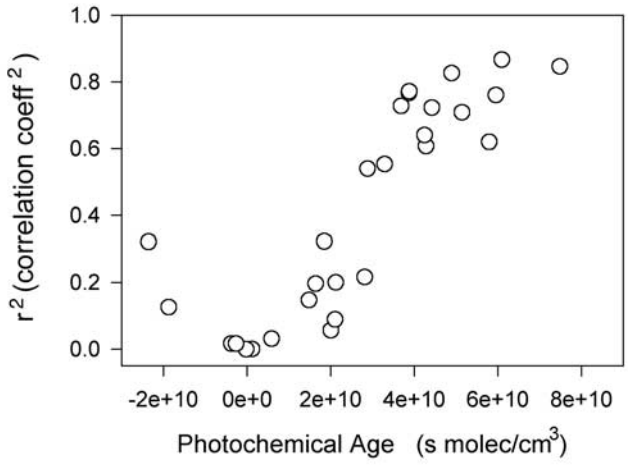

Figure 8. Square of correlation coefficient (r^2) versus photochemical age for the G-1 Urban PM samples. Linear regressions were done using G-1 Urban 1st Quartile as a t = 0 reference point. Note that 4 of the PM samples have a negative photochemical age, indicating less reaction with OH, than occurred in the reference sample.

coincidental as the standard error for the regression slope without reactive olefins is 1.1e10, 50% of the slope.

[35] Figure 6b shows a photochemical age determination for a composite East sample, again using the Downtown surface samples as a t = 0 reference. The East samples are older than the Urban 1st Quartile samples and show significant depletion of moderately reactive alkanes and aromatics. The range of values of $C_i(t)/C_i(0)$ in Figure 6b is much greater than the "noise" level in Figure 6a and the regression without reactive olefins has a respectable degree of correlation ($r^2 = 0.80$). A regression line is not shown for a calculation using reactive olefins as $C_i(t)/C_i(0)$ for those compounds is unrealistically high. This is partly due to a too wide range of k_i and partly due to a reactive olefin artifact in the East samples. Presumably, the Urban 1st Quartile samples are affected by the same artifact, but it is of little consequence because concentrations are much higher.

[36] Figure 7 has photochemical age plots for the oldest and second youngest G-1 East samples, measured relative to the Urban 1st Quartile. Figure 7a is a good example of a case where there is an excellent regression fit ($r^2 = 0.98$). The fit in Figure 7b ($r^2 = 0.43$) is not as good and, at least visually, it appears to be affected by an outlier, toluene. Removing toluene from the regression only changes the slope and intercept by a few percent but significantly increases r^2.

6.2. Correlation Coefficients

[37] Some of the photochemical age regressions have quite high correlation coefficients (e.g., Figure 7a, $r^2 = 0.98$) while others show only marginal correlation (e.g., Figure 6a, $r^2 = 0.20$). It is tempting to concentrate on the high regression coefficient cases as being somehow more valid but this would lead to a serious distortion of the overall data set. Figure 8 shows the relation between photochemical age estimates for the Urban PM samples and r^2, determined from each linear regression. A trend is evident whereby aged samples have high values of r^2 while fresh samples have low values. Higher values of r^2 in aged samples reflect the smaller contribution of a relatively constant measurement noise when the slope is large as illustrated in Figures 6a and 6b.

7. Model Results

[38] Particle trajectory calculations yield the age (time since emission) and number of particles intercepted at a VOC sampling location. In this section we present the particle information in a form that is parallel to our analysis of VOC ratios.

[39] Particle age distributions have been calculated at 84 of the 121 locations where the G-1 VOC samples used in our analysis were taken. The remaining 37 samples were either taken on days where the particle model was not run or were early morning West samples which would require a multiday particle calculation. At each sampling point an age distribution was produced giving the number of particles intercepted with ages resolved to 30 minute time bins. From the age distribution we obtain an average age and a total concentration. Particle calculations were grouped according to geographic location and sampling time as done for the VOCs. The Urban AM group was split into quartiles according to particle concentration. Ages and concentrations were determined for each of the groupings by averaging over individual samples.

[40] Particle age distributions for 4 of the groupings are shown in Figure 9. The average Urban AM and PM samples are seen to have peak contributions from particles in the first 1 or 2 age bins, 0 to 1 h atmospheric transport time. The average East and Mountain samples are located downwind and their ages are progressively older. There is a well-defined delay before particles reach the Mountain sample points. For clarity, we have not included in Figure 9 age distributions for the 4 Urban quartiles. They all have the same shape as the Urban AM average but by construction they vary in concentration. Total concentrations decrease from morning to afternoon due to an increased afternoon

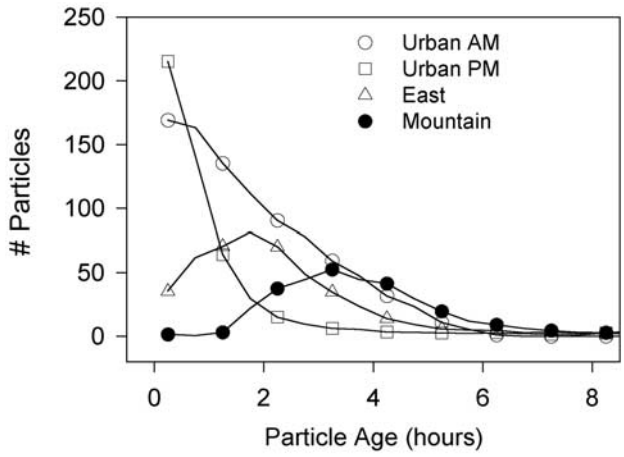

Figure 9. Particle age distribution calculated from PNNL trajectory model. Each curve is generated by averaging over all samples in a subset, giving each sample equal weight. Symbols are shown for every other age bin.

Table 4. Results of Particle Trajectory Calculations With Comparisons to Photochemical Age Calculations and CSS Model Results

		Dilution Factor		Age, h	[OH][a] molec cm^3		
Data Subset	No.	VOC	Particle	Particle	VOC/Particle	CSS (end)[b]	CSS (avg)[c]
Urban 1st Quartile	11	0.40	0.40	1.9	3.5(6)	3.2(6)	2.5(6)
Urban 2nd Quartile	11	0.19	0.22	1.7	6.3(6)	5.7(6)	4.3(6)
Urban 3rd Quartile	11	0.12	0.14	1.7	7.6(6)	9.3(6)	7.4(6)
Urban 4th Quartile	11	0.053	0.035	1.9	1.2(7)	1.0(7)	8.0(6)
Urban PM	20	0.12	0.11	1.2	1.2(7)	7.8(6)	9.5(6)
East	15	0.088	0.10	2.3	1.3(7)	6.8(6)	1.1(7)
Mountain	5	0.068	0.073	4.0	9.0(6)	5.5(6)	1.0(7)

[a]The notation 3.5(6) is meant to be read as 3.5×10^6.
[b]Constrained steady state calculation using conditions at time and place of VOC sample.
[c]Constrained steady state calculation using endpoint concentrations with sample time of day reduced by "Age"/2. This affects solar intensity.

mixing height and wind speed. Concentrations also decrease with distance from the urban center.

[41] Numerical results are reported in Table 4. Comparison is made in the Table to results for the VOC samples. Editing the list of VOC samples to match the smaller number of trajectory calculations produced only small (~10%) nonsystematic changes in the VOC predictions. In the interest of presenting a single set of results, such editing was not done. In order to facilitate a concentration comparison, we have normalized the particle results to give a concentration of 0.40 for the Urban 1st Quartile. This matches the dilution factor calculated from the VOC regression, relative to a t = 0 surface sample. Concentration trends (see "Dilution factor" in Table 4) predicted by the particle model follow those predicted from VOCs. A point-by-point comparison within a geographic subset shows a scattered pattern. Evidently, differences between actual winds and the predicted winds used to drive the trajectory model can displace plumes enough to compromise agreement. This feature was discussed by *Fast et al.* [2000] in their comparison between predicted and observed levels of trace gases in the Phoenix urban plume.

[42] In Table 4 we have divided photochemical age by trajectory age to yield an "inferred" OH concentration (see column, "VOC/Particle"). Comparison is made with OH concentration calculated from a constrained steady state photochemical box model. This comparison is only qualitative because OH predictions from the box model refer to the time and place where measurements are made while the combination of photochemical age and trajectory age yields an average OH experienced by an air parcel.

7.1. Effects of a Spatially Extended Source Region

[43] Emissions in the Phoenix air basin are distributed over a large geographic area and as a consequence VOC samples will contain a mixture of material with different atmospheric residence times. Theory suggests that photochemical age predictions can be distorted [see, e.g., *McKeen et al.*, 1990]. We address this question using the PNNL trajectory model.

[44] As illustrated in Figure 9, the trajectory model produces an age spectrum describing the transport of inert particles from surface emission sources to our sampler in the G-1. An average age, which we term the "trajectory age," is readily calculated. A photochemical age is determined by treating the inert particles as if they were a mixture of reactive VOCs that decay during transport by reaction with a specified concentration of OH. Each particle brings to a virtual receptor canister on the G-1 a mixture of VOCs that are diminished from their initial concentration of unity according to:

$$c_{i,j} = \exp\left(-k_i[OH] \times t_j\right), \tag{9}$$

where t_j is the time it takes the jth particle to travel from the source to the receptor. The total concentration of each VOC at the receptor is determined as the sum of contributions from all particles collected at the receptor,

$$C_i = \sum_j c_{i,j}. \tag{10}$$

[45] The calculation of VOC concentrations from the particle model is illustrated in Figure 10. The top curve shows the particle distribution for an unreactive tracer

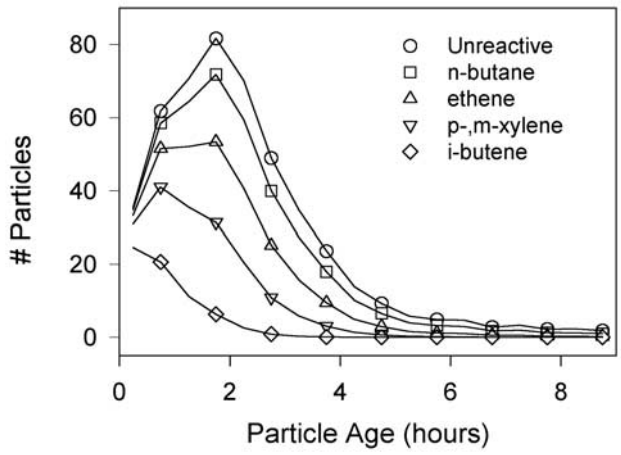

Figure 10. Distribution of particle age for particles that react with OH. Top curve shows particle age distribution for an average East sample in the absence of reaction. Other curves are calculated assuming that particles react with OH with rate constants appropriate to either n-butane, ethene, p-, m-xylene or i-butene (see equations (9) and (10)). OH concentration is set at 8×10^6 cm^{-3}. Symbols are shown for every other age bin.

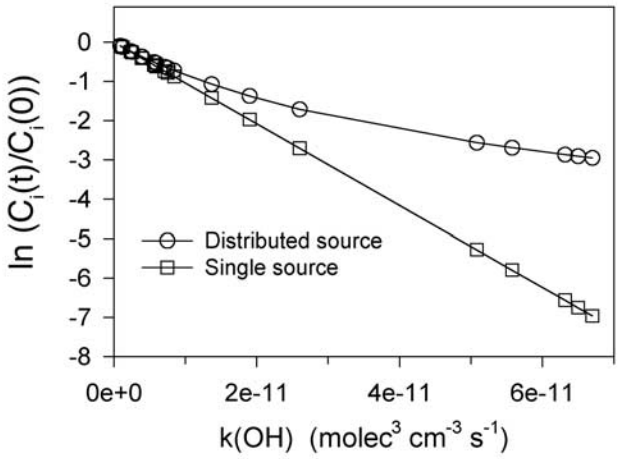

Figure 11. Photochemical age regression plots of ln (VOC ratio) versus OH reaction rate constant. "VOC" concentrations are calculated from reactive particle model for a composite East sample. Particles react with an OH concentration of 1.25×10^7 cm^{-3}, with rate constants equal to the VOC rate constants. Square symbols show the decay in VOC concentration assuming that all particles are emitted from a single point source located 2.31 hour away from the composite East sample. Circles show the decay in VOC concentration calculated using the actual particle trajectories, which take into account the spatially distributed emission source. Points have been connected with straight lines. Regression slopes are reported in text.

which is used to determine the "true" trajectory age. Other curves indicate how that spectrum is diminished and shifted to younger ages as species reactivity increases. In contrast to the unreactive tracer or the less reactive alkanes, iso-butene is seen to peak in the lowest age bins indicating that this VOC is predominately coming from nearby sources. A photochemical age determination that relied on iso-butene would yield a large underestimate for the photochemical age of the entire mix of hydrocarbons.

[46] Total concentrations of each VOC (ie, C_i) have been calculated from (9–10). As with the VOCs, a regression of ln (C_i) versus k_i yields a photochemical age. Figure 11 is an example constructed for an averaged East sample using an assumed OH concentration of 1.25×10^7 cm^{-3}. We also show for comparison the set of data points that would result if all emissions were coming from a single source with travel time equal to the trajectory age. The latter points lie on a straight line. For the spatially distributed source, data points have a distinct upward curvature so that a least squares regression fit will depend on the set of VOCs that are used. In this example we get a photochemical age of 1.04×10^{11} s cm^{-3} for the single source and ages of 4.8×10^{10} and 8.1×10^{10} s cm^{-3} for the spatially distributed source with and without reactive olefins, respectively. Thus, there is an underestimate of photochemical age for the spatially distributed source which becomes more severe when faster reacting VOCs are used.

[47] Similar calculations have been done for each of the 84 virtual particle samples. Table 5 shows the resulting underestimates in photochemical age averaged over geographic subsets, for assumed OH concentrations ranging from 2.5×10^6 to 1.5×10^7 cm^{-3}. Equation (5) suggests that high OH concentration degrades the accuracy of a photochemical age prediction in agreement with Table 5.

8. Discussion

[48] The geographic and temporal trends in photochemical age and dilution factor are in qualitative agreement with the picture that the downtown area is a major source region and that samples collected to the east are capturing material that has undergone mixing and photochemical aging. Case studies by *Fast et al.* [2000] support this picture. However, the emission region is geographically disperse (Figure 1) so that VOCs collected in East and Mountain samples are not necessarily transported from a central downwind location. There is a very high variability in dilution factor within data subsets, which is due to multiple source regions with different emission rates. Because of the multiplicity of source regions, our sample groups cannot be arranged in a time sequence that parallels the time evolution of the urban plume. Thus, Urban, East, and Mountain samples do not necessarily represent 3 stages in the time evolution of the urban plume, though on some days this is true. A better description of our sampling strategy is that we are characterizing several regions that are geographically located in the general direction of plume transport.

[49] The Phoenix area with its geographically distributed emission sources presents a stringent test of the photochemical age methodology. Results presented in Table 5 indicate that the spatial distribution of emission sources can introduce a 10 to 30% underestimate of photochemical age for the various Phoenix data subsets. This range is based on the OH concentrations presented in Table 4; a 10% error being appropriate for the Urban 1st Quartile samples and a 30% error appropriate for Urban PM and East samples. Errors could be reduced significantly by restricting the reactivity range of VOCs, but at the expense of less robust regressions. Another approach developed by *Rudolph and Czuba* [2000] is to make use of the kinetic isotope effect for reactions of ^{12}C and ^{13}C VOCs with OH. Reactivity differences are small, guaranteeing that the condition expressed by (5) is always satisfied. Because the reactivity difference is small a very precise determination of ^{12}C to ^{13}C ratio is required. Dilution factors are less susceptible to systematic error as compared with photochemical age. There is reasonable agreement between dilution factors obtained from the intercept of a VOC regression and the particle model.

[50] Table 4 shows that OH concentrations inferred from a combination of photochemical age and trajectory age (hereinafter called inferred OH) are generally higher than

Table 5. Effect of Spatial Distribution of Emission Sources on Photochemical Age Predictions

	Age Ratio (Spatially Distributed/Single Location)			
[OH], molec cm^{-3}	Urban AM	Urban PM	East	Mountain
2.5e6	0.93	0.90	0.93	0.95
5.0e6	0.86	0.83	0.88	0.91
7.5e6	0.81	0.78	0.83	0.88
1.0e7	0.76	0.75	0.79	0.85
1.25e7	0.71	0.71	0.75	0.82
1.5e7	0.67	0.69	0.72	0.79

the OH obtained from a constrained steady state (CSS) photochemical model. Agreement is better in the morning than afternoon. The CSS model predicts the OH trends inferred for the Urban Quartiles, namely that OH concentrations decrease as pollutant levels increase. Inferred OH in the 4th Quartile is 3.4 times that in the 1st Quartile; calculated OH increases by a factor of 3.2. A decrease in OH at high NO_x concentration is expected because of $OH + NO_2 \rightarrow HNO_3$ [see, e.g., *Logan et al.*, 1981].

[51] An exact correspondence between inferred and calculated OH was not expected as the inferred OH is an average value over a several hour trajectory while the calculated OH is an instantaneous value at the end of the trajectory. This is of particular concern for the East and Mountain samples which were collected late in the afternoon under low solar intensity conditions. Changing the time of day in the CSS calculation to correspond to the midpoint of the trajectory increases the calculated OH for the afternoon samples and even results in a small overprediction for the Mountain samples. However, this effect works in the opposite direction for the morning samples and increases the disparity. When time of-day-effects are taken into account the average morning and afternoon predicted OH are, respectively, 74 and 91% of inferred, based on an equal weighting for each subset. Our calculations do not take into account the changing chemical conditions along a trajectory, which are difficult to estimate without doing a detailed time dependent calculation.

[52] The regression methodology used in this study to derive a photochemical age closely resembles that used by *Volz-Thomas and Kolahgar* [2000] for the Schauinsland Ozone Precursor Experiment (SLOPE96). In that study, inferred OH was approximately 2 times higher than OH obtained from a photochemical calculation that took into account the changes along a trajectory. SLOPE96 results pertain to high NO_x conditions such as exist in about half of the Phoenix Urban AM samples. Our OH predictions show somewhat better agreement. However, we have not taken into account results from Table 5 indicating that there is a systematic 10 to 30% underestimate in photochemical age due to the spatial distribution of emission sources. Also, effects of changing chemical conditions along a trajectory remain un-quantified. In looking for a cause for our likely underprediction of OH we have to consider the possibility of errors in the wind fields and trajectory calculations, in addition to errors in chemistry. Unlike the SLOPE96 experiment, we don't have a tracer (SF_6) to document transport.

9. Conclusions

[53] We have used VOC measurements obtained during a late spring field campaign in the Phoenix air basin to obtain photochemical age estimates. Morning surface observations in Downtown Phoenix provide a VOC speciation for fresh emissions. VOC observations were made by the G-1 aircraft at midboundary layer height and at a downwind surface site located in Usery Pass. Relative to the downtown surface observations, the G-1 and Usery Pass measurements indicate the selective disappearance of reactive VOCs due to OH chemistry and a nonselective decrease in concentrations due to mixing of source air with clean background air. Photochemical age was determined from a linear regression method that considered 15 VOCs with reactivity varying between acetylene and p,m-xylene. We show that photochemical ages can be combined by addition and dilution factors by multiplication. Effects of measurement error and/or variable source type are seen in the regression coefficients, which decrease at low photochemical age. A 25 to 30% uncertainty in photochemical age is estimated from the regression statistics.

[54] Photochemical age calculations indicate that older more dilute samples are found to the east of Phoenix, a trend that agrees with the qualitative picture of west to east transport of the urban plume. The downwind surface site at Usery Pass had a pronounced diurnal cycle in photochemical age with nearly fresh emissions observed in the early morning (0100–0400) and a well aged mixture observed between 1000 and 1600. Photochemical age estimates at 1 km above the surface agree well with the Usery Pass results.

[55] The PNNL particle trajectory model was used to simulate the atmospheric fate of reactive VOCs by following particles that are released from the surface in proportion to a NO_x emission rate. Subjecting the trajectory model output to the same methodology used to calculate photochemical age, we find that the photochemical ages of the G-1 samples are underestimated by 10 to 30% due to the circumstance that each G-1 sample contains VOCs with a broad distribution of atmospheric residence times. In agreement with published numerical and analytic results we find that underestimates become larger when more reactive compounds are used to estimate age. Reactive olefins (propene and more reactive compounds) are only useful for samples that have undergone little aging.

[56] Dividing the photochemical age (determined from VOC ratios) by an average particle transport time (determined from the particle trajectory model) yields a prediction of OH concentration (inferred OH). For a qualitative comparison, a photochemical box model was used to predict the concentration of OH that is in equilibrium with the observed mixture of stable trace gasses. Inferred OH is a few 10s of percent higher than calculated OH, but for the most part these two measures have the same trends.

[57] **Acknowledgments.** We thank the pilots and flight crew from PNNL for a job well done. We gratefully acknowledge the many contributions of Paul Klotz of BNL, and John Hubbe and Victor Morris of PNNL in collecting and reducing the data. The continued support of the Atmospheric Chemistry Program within the Office of Biological and Environmental Research of DOE is greatly appreciated. We thank Danny Wang from the Analytical and Air Quality Division of Environment Canada (Ottawa) for supplying the reference gases for calibration of the York University NMHC measurements. Judith Weinstein-Lloyd acknowledges support from NSF award ATM-9414108 and DOE award DE-FG02-98ER62586. This research was performed under sponsorship of the U.S. DOE under contracts DE-AC02-98CH10886.

References

Apel, E. C., J. G. Calvert, and F. C. Fehsenfeld, The nonmethane hydrocarbon intercomparison experiment (NOMHICE): Tasks 1 and 2, *J. Geophys. Res.*, *99*, 16,651–16,664, 1994.

Apel, E. C., J. G. Calvert, T. M. Gilpin, F. C. Fehsenfeld, D. D. Parrish, and W. A. Lonneman, The Nonmethane Hydrocarbon Intercomparison Experiment (NOMHICE), Task 3, *J. Geophys. Res.*, *104*, 26,069–26,086, 1999.

Atkinson, R., Gas-phase tropospheric chemistry of organic compounds, *J. Phys. Chem. Ref. Data*, *Monograph 2*, 1–216, 1994.

Blake, N. J., S. A. Penkett, K. C. Clemitshaw, P. Anwyl, P. Lightman, A. R. W. Marsh, and G. Butcher, Estimates of atmospheric hydroxyl radical

concentrations from the observed decay of many reactive hydrocarbons in well-defined urban plumes, *J. Geophys. Res.*, *98*, 2851–2864, 1993.
Calvert, J. G., Hydrocarbon involvement in photochemical smog formation in Los Angeles atmosphere, *Environ. Sci. Technol.*, *10*, 256–262, 1976.
Cowling, E. B., W. L. Chameides, C. S. Kiang, F. C. Fehsenfeld, and J. F. Meagher, Introduction to special section: Southern Oxidants Study Nashville/Middle Tennessee Ozone Study, *J. Geophys. Res.*, *103*, 22,209–22,212, 1998.
Cowling, E. B., W. L. Chameides, C. S. Kiang, F. C. Fehsenfeld, and J. F. Meagher, Introduction to special section: Southern Oxidants Study Nashville/Middle Tennessee Ozone Study, Part 2, *J. Geophys. Res.*, *105*, 9075–9077, 2000.
Doskey, P. V., J. Rudolph, and R. Kotamarthi, Measurements of nonmethane hydrocarbons in Phoenix, Arizona, in *Symposium on Atmospheric Chemistry Issues in the 21st Century*, *Preprints*, pp. 30–32, Am. Meteorol. Soc., Long Beach, Calif., 2000.
Ehhalt, D. H., F. Rohrer, A. Wahner, M. J. Prather, and D. R. Blake, On the use of hydrocarbons for the determination of tropospheric OH concentration, *J. Geophys. Res.*, *103*, 18,981–18,997, 1998.
Ellis, W. A., M. L. Hildebrandt, and H. J. S. Fernando, Evidence of lower-atmosphere ozone "sloshing" in an urbanized valley, *Phys. Geograph.*, *20*, 520–536, 1999.
Environmental Protection Agency (EPA), Technical Assistance Document for Sampling and Analysis of Ozone Precursors, *Rep. No. EPA/600-8-91/215*, Research Triangle Park, N.C., 1991.
Environmental Protection Agency (EPA), National Air Quality and Emissions Trends Report, 1998, *Rep. No. EPA/454/R-00-003*, Research Triangle Park, N.C., 2000.
Fast, J. D., and C. M. Berkowitz, A modeling study of boundary layer processes associated with ozone layers observed during the 1993 North Atlantic Regional Experiment, *J. Geophys. Res.*, *101*, 28,683–28,699, 1996.
Fast, J. D., J. C. Doran, W. J. Shaw, R. L. Coulter, and T. J. Martin, The evolution of the boundary layer and its effect on air chemistry in the Phoenix area, *J. Geophys. Res.*, *105*, 22,833–22,848, 2000.
Fukui, Y., and P. V. Doskey, An enclosure technique for measuring nonmethane organic compound emissions from grasslands, *J. Environ. Qual.*, *25*, 601–610, 1996.
Gaffney, J. S., N. A. Marley, P. J. Drayton, P. V. Doskey, R. V. Kotamarthi, M. M. Cunningham, J. C. Baird, J. Dintamen, and H. L. Hart, Field observations of regional and urban impacts on NO_2, ozone, and nitrate radical production rates in the Phoenix air basin, *Atmos. Environ.*, *36*, 825–833, 2002.
Heisler, S. L., P. Hyde, M. Hubble, F. Keene, G. Neuroth, M. Ringsmuth, and W. R. Oliver, Reanalysis of the Metropolitan Phoenix early ozone plan (VEOP), ENSR Document 0493-014-710, ENSR Consult. and Eng., Camarillo, Calif., 1997.
Kleinman, L. I., P. H. Daum, J. H. Lee, Y.-N. Lee, L. J. Nunnermacker, S. R. Springston, L. Newman, J. Weinstein-Lloyd, and S. Sillman, Dependence of ozone production on NO and hydrocarbons in the troposphere, *Geophys. Res. Lett.*, *24*, 2299–2302, 1997.
Logan, J. A., M. J. Prather, S. C. Wofsy, and M. B. McElroy, Tropospheric chemistry: A global perspective, *J. Geophys. Res.*, *86*, 7210–7254, 1981.
Madronich, S., Photodissociation in the atmosphere, 1, Actinic flux and the effects of ground reflections and clouds, *J. Geophys. Res.*, *92*, 9740–9752, 1987.
McKeen, S. A., and S. C. Liu, Hydrocarbon ratios and photochemical history of air masses, *Geophys. Res. Lett.*, *20*, 2363–2366, 1993.
McKeen, S. A., M. Trainer, E.-Y. Hsie, R. K. Tallamraju, and S. C. Lin, On the indirect determination of atmospheric OH radical concentrations from reactive hydrocarbon measurements, *J. Geophys. Res.*, *95*, 7493–7500, 1990.
McKeen, S. A., S. C. Liu, E.-Y. Hsie, X. Lin, J. D. Bradshaw, S. Smyth, G. L. Gregory, and D. R. Blake, Hydrocarbon ratios during PEM-West(A): A model perspective, *J. Geophys. Res.*, *101*, 2087–2109, 1996.
McKenna, D. S., Analytic solutions of reaction diffusion equations and implications for the concept of an air parcel, *J. Geophys. Res.*, *102*, 13,719–13,725, 1997.
McKenna, D. S., C. J. Hord, and J. M. Kent, Hydroxyl radical concentrations and Kuwait oil fire emission rates for March 1991, *J. Geophys. Res.*, *100*, 26,005–26,025, 1995.
Parrish, D. D., C. J. Hahn, E. J. Williams, R. B. Norton, F. C. Fehsenfeld, H. B. Singh, J. D. Shetter, B. W. Gandrud, and B. A. Ridley, Indications of photochemical histories of Pacific air masses from measurements of atmospheric trace species at Point Arena, California, *J. Geophys. Res.*, *97*, 15,883–15,901, 1992.
Parrish, D. D., et al., Internal consistency tests for evaluation of measurements of anthropogenic hydrocarbons in the troposphere, *J. Geophys. Res.*, *103*, 22,339–22,359, 1998.
Paulson, S. E., and J. H. Seinfeld, Development and evaluation of a photochemical mechanism for isoprene, *J. Geophys. Res.*, *97*, 20,703–20,715, 1992.
Ramacher, B., J. Rudolph, and R. Koppmann, Hydrocarbon measurements in the spring arctic troposphere during the ARCTOC 95 campaign, *Tellus*, *49B*, 466–485, 1997.
Roberts, J. M., F. C. Fehsenfeld, S. C. Liu, M. J. Bollinger, C. Hahn, D. L. Albritton, and R. E. Sievers, Measurements of aromatic hydrocarbon ratios and NO_x concentrations in the rural troposphere: Observation of air mass photochemical aging and NO_x removal, *Atmos. Environ.*, *18*, 2421–2432, 1984.
Rudolph, J., Measurements of nonmethane hydrocarbons in the atmosphere, in *Volatile Organic Compounds in the Troposphere*, edited by R. Koppmann and D. H. Ehhalt, pp. 11–35, vol. 16, Schriften des Forschungszentrum Jülich Reihe Umwelt/Environment, 1999.
Rudolph, J., and A. Khedim, Hydrocarbons in the nonurban atmosphere: Analysis, ambient concentrations and impact on the chemistry of the atmosphere, *Int. J. Environ. Anal. Chem.*, *20*, 265–282, 1985.
Rudolph, J., and F. J. Johnen, Measurements of light hydrocarbons over the Atlantic in regions of low biological activity, *J. Geophys. Res.*, *95*, 20,583–20,591, 1990.
Rudolph, J. E., and E. Czuba, On the use of isotopic composition measurements of volatile organic compounds to determine the "photochemical age" of an air mass, *Geophys. Res. Lett.*, *27*, 3865–3868, 2000.
Satsumabayashi, H., H. Kurita, Y.-S. Chang, G. R. Carmichael, and H. Ueda, Diurnal variations of OH radical and hydrocarbons in a polluted air mass during long-range transport in central Japan, *Atmos. Environ.*, *26A*, 2835–2844, 1992.
Solomon, P., E. Cowling, G. Hidy, and C. Furiness, Comparison of scientific findings from major ozone field studies in North America and Europe, *Atmos. Environ.*, *34*, 1885–1920, 2000.
Stockwell, W. R., P. Middleton, J. S. Chang, and X. Tang, The second generation regional acid deposition model chemical mechanism for regional air quality modeling, *J. Geophys. Res.*, *95*, 16,343–16,367, 1990.
Volz-Thomas, A., and B. Kolahgar, On the budget of hydroxyl radicals at Schauinsland during the Schauinsland Ozone Precursor Experiment (SLOPE96), *J. Geophys. Res.*, *105*, 1611–1622, 2000.

C. Berkowitz and J. Fast, Atmospheric Sciences Department, Pacific Northwest National Laboratory, Richland, WA 99352, USA. (Carl.Berkowitz@pnl.gov; Jerome.Fast@pnl.gov)

P. Daum, L. I. Kleinman, Y.-N. Lee, L. J. Nunnermacker, and S. R. Springston, Atmospheric Sciences Division, Brookhaven National Laboratory, Upton, NY 11973, USA. (phdaum@bnl.gov; kleinman@bnl.gov; ynlee@bnl.gov; lindan@bnl.gov; srs@bnl.gov)

P. Doskey, Environmental Research Division, Argonne National Laboratory, Argonne, IL 60439, USA. (pvdoskey@anl.gov)

P. Hyde, Air Quality Division, Arizona Department of Environmental Quality, 3003 North Central Avenue, Phoenix, AZ 85012, USA. (Hyde.Peter@ev.state.az.us)

J. Rudolph, Chemistry Department and Centre for Atmospheric Research, York University, Toronto, Ontario M3J 1P3, Canada. (rudolphj@yorku.ca)

J. Weinstein-Lloyd, Chemistry/Physics Department, SUNY/Old Westbury, Old Westbury, NY 11568, USA. (jlloyd@bnl.gov)